J. Fluid Mech. (1989), *vol.* 205, *pp.* 45–76
Printed in Great Britain

Turbulence structure of a boundary layer beneath a turbulent free stream

By P. E. HANCOCK† AND P. BRADSHAW‡
Department of Aeronautics, Imperial College, London SW7 2BY, UK

(Received 18 January 1988 and in revised form 3 February 1989)

Measurements have been made in the turbulent boundary layer on a flat plate in the presence of grid-generated free-stream turbulence with a wide range of lengthscales. The data include conditionally sampled averages in which free-stream fluid was distinguished from boundary-layer fluid by heating the latter. Free-stream turbulence increases the standard deviation of the hot–cold interface as a proportion of the boundary-layer thickness, whilst the average position is mainly dependent upon the lengthscale. The shear correlation coefficient of the boundary-layer fluid decreases, and it is shown that the change in structure is directly related to the fluctuating-strain rate.

Transport velocities representing the diffusion of turbulent kinetic energy and shear stress have opposite signs in the boundary-layer fluid to those in the free-stream fluid, and it is shown that they are also related to the fluctuating-strain rate.

Complete balances of turbulent kinetic energy and shear stress have been evaluated, dissipation and pressure–strain redistribution having been deduced by difference. The dissipation length scale $L_\tau = (-\overline{uv})^{\frac{3}{2}}/\epsilon$ is little affected by free-stream turbulence, whereas the corresponding parameter based on turbulent energy instead of shear stress is strongly affected.

1. Introduction

This paper is one of a series on complex turbulent flows (defined as shear layers with complicating influences like distortion by extra rates of strain or interaction with another turbulence field). Other members of the series concerned with the interaction between two shear layers include the papers by Dean & Bradshaw (1976), Weir, Wood & Bradshaw (1981) and Andreopoulos & Bradshaw (1980). In the present paper, we discuss the interaction between a turbulent boundary layer and an external stream that has turbulence but no significant mean shear. The object of the work is to provide inspiration for calculation methods suitable for the prediction of development of turbulent boundary layers or other shear layers in arbitrary pressure gradients and with arbitrarily anisotropic free-stream turbulence. However, in common with most previous investigators, we have chosen to study the response of a boundary layer in zero pressure gradient to nearly isotropic free-stream turbulence, on the argument that any well-founded calculation method should be able to cope with the extra complication of non-zero pressure gradient, and that the effect of mild anisotropy might be inferrable. Strongly anisotropic free-stream 'turbulence' occurs only when the free stream contains significant mean shear or inhomogeneity as in

† Present address, University of Surrey, Guildford, Surrey GU2 5XH, UK.
‡ Present address, Stanford University, Stanford, California, CA 94305, USA.

turbomachinery where blade wakes constitute ordered unsteadiness as well as turbulence.

Many previous workers have studied the response of mean-flow parameters, especially skin-friction coefficients, to free-stream turbulence: for a review see Hancock (1980), summarized by Hancock & Bradshaw (1983, hereinafter referred to as I). More recent measurements than reviewed by I are given by Blair & Edwards (1982), Blair (1983), and Castro (1984). Rodi & Scheuerer (1985) have compared the measurements of Hancock and Blair & Edwards with predictions based on transport equations for the Reynolds stresses and dissipation, and also on transport equations for the turbulent kinetic energy and dissipation. Comparatively few measurements of the turbulence have been made, partly because of the inherent difficulty in distinguishing the contribution of the free stream, and of the boundary layer itself, to the turbulence within the nominal boundary layer. In the present work we have used 'conditional sampling' techniques to distinguish between free-stream fluid and boundary-layer fluid, by slightly heating the boundary layer near the leading edge of the plate on which it is formed. The instantaneous boundary between the heated and the unheated fluid is nominally coincident with the outer boundary of a plume of smoke introduced near the flow origin, and although the fluctuations within the 'hot' region undoubtedly receive contributions from the pressure-fluctuation field generated by the free-stream turbulence, the contaminant boundary can be justifiably regarded as the boundary between eddy motions generated in the sheared boundary layer and those generated by the turbulence grid. This distinction is implicit in most calculation methods for turbulent boundary layers beneath turbulent free streams, and would seem to be a unique and rigorous one, at least for fluids with molecular Prandtl number near unity. The 'hot–cold' discrimination techniques, and the statistical processing, were essentially the same as those used successfully in interactions between two shear layers by Weir *et al.*

It was pointed out in I that the conclusions of previous workers, that the effect of free-stream turbulence depended mainly upon its intensity and very little upon its lengthscale, arose from the restricted range of previous experiments. Briefly, the relatively small range of sizes and speeds of wind tunnels used in basic research, together with the near-unanimity of previous workers on the need to avoid making measurements too close to a turbulence grid, or at too small a boundary-layer Reynolds number have confined measurement conditions almost to a straight line in the 'intensity–lengthscale' plane: the effects of two variables cannot be distinguished if one is always proportional to the other. The present work, a continuation of that reported in I, appears to be the first in which a positive attempt has been made to cover a large area in the intensity–lengthscale plane, and it is also the first in which conditional-sampling techniques have been used, with the exception of the work of Charnay, Mathieu & Comte-Bellot (1976). However, even allowing for their lower Reynolds number, the frequency response of their temperature probe was apparently too low to resolve the fine structure of the hot–cold interface, which as shown here is even more irregular than the turbulent–non-turbulent interface in an ordinary shear layer.

Rodi & Scheuerer found, not surprisingly, that their Reynolds-stress transport calculation gave the better results of the two methods, showing broadly the correct changes with intensity, but with the opposite effect of lengthscale to that observed. The latter shortcoming is undoubtedly due, at least in part, to a larger eddy viscosity at the larger lengthscale in the implied eddy-viscosity relationship near the boundary-layer edge, and to the failure to correctly model the effect of the wall on

the external turbulence. A larger eddy viscosity arises because of the smaller dissipation at the larger lengthscale.

This paper is a fuller version of Hancock & Bradshaw (1987).

2. Experimental techniques

The measurements were made in a $0.91 \times 0.91 \times 4.9$ m-long low-turbulence wind tunnel at a speed of about 16.5 m s^{-1}. Square-mesh square-bar 'biplane' grids with mesh lengths, M, of 76 mm and 152 mm were mounted at the front of the working section, and the measurements were made on a 2.4 m-long flat plate with an ogive-shaped leading edge (to reduce instantaneous separation) suspended in the middle of the tunnel. Biplane grids, with the horizontal and vertical sets of bars touching but not intersecting, were found to give a more stable and homogeneous, isotropic turbulence field, and better spectral distribution, than grids with both sets of bars in the same plane, biplane grids of rectangular bars, or grids of a single row of bars. Turbulence intensities, and the ratio of free-stream lengthscale to the boundary-layer thickness, were varied by changing the size of the grid, the distance of the plate leading edge from the grid, and the distance of the measuring station from the plate leading edge. The maximum intensity allowed at the plate leading edge was $(u'/U)_e = 15\%$, where u' denotes the r.m.s. of the streamwise velocity fluctuation, u, and U is the streamwise mean velocity. Suffix 'e' is used throughout to denote conditions in the free stream, which is defined formally in §3.2. The maximum intensity at any measurement station was $(u'/U)_e = 6\%$ because of our further requirement that the distance of a measuring station from the plate leading edge should be large enough for the momentum-thickness Reynolds number to exceed 2000. All three velocity fluctuation components, and their spectra, have been measured in the free stream. For ease of comparison with the many experiments in which only the longitudinal-component intensity behind a turbulence grid was measured, we have defined the free-stream turbulence lengthscale, L_e^u, by the equation

$$U_e \frac{\mathrm{d}(\overline{u^2})_e}{\mathrm{d}X} = \frac{-(\overline{u^2})_e^{\frac{3}{2}}}{L_e^u}, \tag{1}$$

where X is the distance from the grid. If the turbulence were isotropic the left-hand side would be two-thirds of the rate of turbulent energy dissipation. L_e^u was determined from (1) and a power-law fit of $(\overline{u^2})_e$ as a function of the form $(X-X_0)^{-n}$ where for the present grids a value of $n = 1.25$ was used. In the absence of a turbulence grid the free-stream intensity $(u'/U)_e$ was 0.03% – hereafter denoted as 'zero'.

Mean velocity measurements were made with conventional Pitot tubes of diameter about 1 mm, and skin-friction coefficients were deduced from logarithmic plots on the assumption that the universal logarithmic law applies in the presence of free-stream turbulence – an assumption made by most previous workers, but for which the present turbulence measurements, to be discussed below, provide almost the first experimental justification. Velocity fluctuations were measured with crossed hot wires, with wire lengths of about 1 mm, driven by Disa constant-resistance bridges. Temperature fluctuations were measured with a 1 mm-long 1 μm diameter wire, operated at a constant current of about 1 mA, compensated for thermal inertia by a homemade amplifier circuit, and mounted about 1 mm to one side of the crossed-wire array, outside the hot-wire wakes.

Resistance-thermometer compensation was set by observing the output trace in an intermittently 'hot' region of the flow, and adjusting the time constant of the compensation so that, at the end of a hot interval, the temperature decreased to the 'cold' free-stream level as rapidly as possible without overshoot: the frequency response was estimated to be about 10 kHz, corresponding to a streamwise wavelength of 1.5 mm in a flow at 15 m s^{-1}. This length was about equal to the spatial resolution length of the three-wire probe. The effect of velocity fluctuations on the temperature signal, easily checked by observing the signal from the temperature probe in the absence of heating, was found to be negligible. The effect of mean and instantaneous temperature changes on the velocity fluctuation measurements was subtracted during signal processing. All fluctuating signals were recorded on analogue magnetic tape during the experiments, and later digitized (at $\sim$ 16 kHz sampling rate for the conditionally sampled analysis) for batch processing at the College computer centre. The hot–cold discrimination was primarily based on a significant rise of the measured temperature above the background cold level, with allowance for slow variations of the cold level with time, and with the additional safeguard that cold bursts were also declared if the time derivative of temperature became large (and negative). The level and gradient thresholds were set by observation of a large number of calcomp plots samples so as to give an intermittency function that was considered an acceptable interpretation of the temperature signal. No attempt was made to force agreement with the results of previous workers. For further details of the intermittency algorithm, thresholds and a representative sample of plots see Hancock (1980). Charnay *et al.* (1976) obtained the intermittency function by means of analogue electronics which do not have the advantages possessed by digital processing.

3. Results and discussion

3.1. *Free-stream turbulence and mean flow*

The measurements presented here were made with the plate leading edge positioned 300 mm downstream of the 76 mm-mesh grid and at 760, 1370 and 2060 mm downstream of the 152 mm-mesh grid. At the various measuring positions the lateral fluctuation intensities v' and w' were between 2% and 5% less than the longitudinal intensity u', the intensity ratios varying only slowly with X. Sample one-dimensional spectra of u, v, w, respectively, ϕ_u, ϕ_v, ϕ_w, are shown in figure 1. (The Taylor microscale was about 230 for the larger grid.) The u-component mean-square intensities were well fitted by

$$[\overline{u^2}/U^2]_e = 0.0476\ (X/M - 4.81)^{-1.25} \tag{2}$$

and

$$[\overline{u^2}/U^2]_e = 0.0700\ (X/M - 3.65)^{-1.25} \tag{3}$$

for the 76 mm and 152 mm grids, respectively.

Figure 2 shows the free-stream intensities $(u'/U)_e$ and length-scale ratios (L_e^u/δ_{995}) at which the detailed turbulence measurements were made. δ_{995} is the boundary-layer thickness defined by $U = 0.995U_e$. Some further details are given in table 1. (The letters displayed in table 1 and figure 2 correspond to those employed in I. The parameter β in figure 2 is defined below.) Lines joining the points in cases E and C indicate that these data were obtained at different positions along the plate with the plate at a fixed distance downstream of the grid. Most of the data presented here are from cases F, E2, C3, E1, G and H – i.e. two length-scale ratios at each of three free-

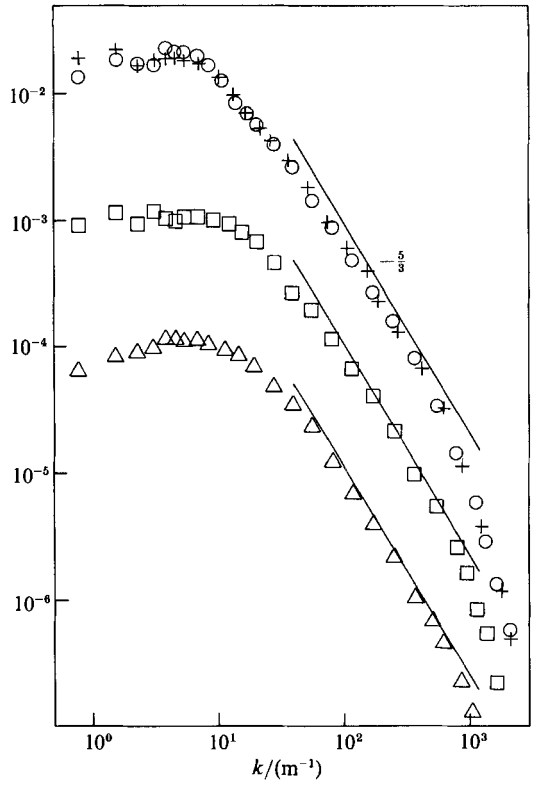

FIGURE 1. Sample free-stream spectra $\phi_u(k)$, $\phi_v(k)$, $\phi_w(k)$ at $X/M = 23.5$ from 152 mm grid. ○, +, $\phi_u/\overline{u_e^2}$; □, $\phi_v \times 10^{-1}/\overline{v_e^2}$; △, $\phi_w \times 10^{-2}/\overline{w^2}_e$. k is the wavenumber.

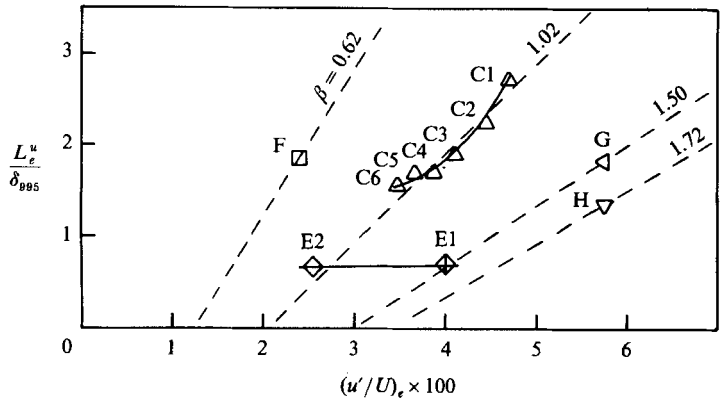

FIGURE 2. Values of $(u'/U)_e$ and L_e^u/δ_{995} for detailed turbulence measurements. F, E2, etc. are case identifiers and correspond to data in table 1. Broken lines are lines of β = constant.

stream intensities of approximately 2.5 %, 4.0 %, and 5.8 %. Unless otherwise stated, the symbols used in figure 2 will be used in other figures to denote $(u'/U)_e$ and L_e^u/δ_{995}.

Profiles of mean velocity are shown in figure 3, the remainder of set C being give in I. The apparent near self-preservation of the mean flow and some turbulence quantities in set C is fortuitous and is caused by the opposite, and in this case

Symbol	x	$(u'/U)_e$	L_e^u/δ_{995}	δ_{995}	C_f	$U_e\theta/\nu$	δ_{05}/δ_{995}	$\bar{y}/\delta_{995}$	σ/δ_{995}
			No free-stream turbulence						
○	910	(0.0003)	—	22.7	0.00316	2870	0.94	0.90	0.13
+	2130	(0.0003)	—	38.7	0.00296	4680	0.94	0.90	0.13
			Case F ($X_{LE} = 2060$, $M = 76$)						
□	910	0.024	1.88	29.1	0.00344	2980	0.93	0.81	0.23
			Cases E1 and E2 ($X_{LE} = 305$, $M = 76$)						
◈	1220	0.040	0.71	56.9	0.00368	3710	0.96	0.97	0.42
◇	2430	0.026	0.67	78.4	0.00325	5760	0.91	0.94	0.42
			Cases C2, C3 and C5 ($X_{LE} = 2060$, $M = 152$)						
◭	1220	0.044	2.23	46.4	0.00352	3750	1.03		
△	1520	0.041	1.90	56.8	0.00339	4320	1.04	0.76	0.43
◭	2130	0.036	1.69	68.9	0.00326	5240	1.14		
			Case G ($X_{LE} = 1370$, $M = 152$)						
◁	910	0.058	1.83	48.1	0.00382	3100	1.05	0.71	0.44
			Case H ($X_{LE} = 760$, $M = 152$)						
▽	1520	0.058	1.34	66.0	0.00376	3860	1.45	1.19	0.83

TABLE 1. Details of profile sets. (Dimensions in mm.) x = distance from the plate leading edge. X_{LE} = distance of leading edge from grid.

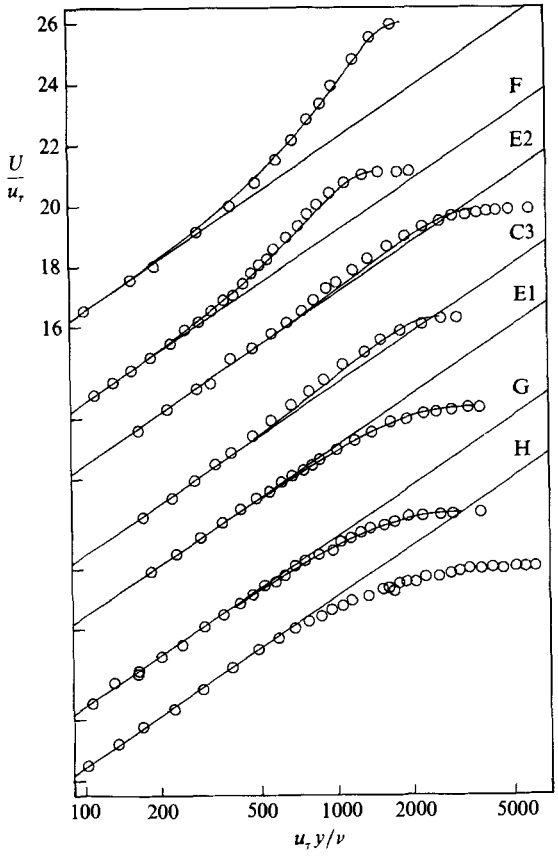

FIGURE 3. Mean velocity profile in logarithmic, law-of-the-wall coordinates. Top profile is for $u'_e = 0$ ($x = 2130$ mm): other cases are identified in table 1. ——, Wake function of Dean (– see I).

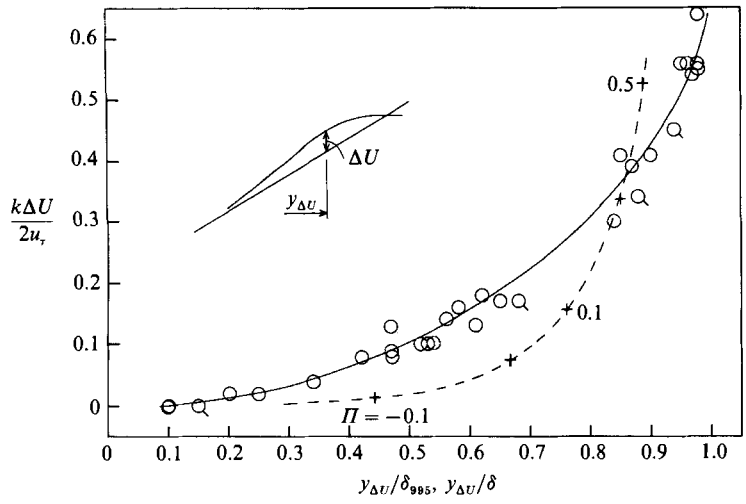

FIGURE 4. Maximum positive departure, ΔU, of outer-layer velocity profile from logarithmic-law behaviour for various $(u'/U)_e$ and L_e^u/δ_{995}. (Some data from I.) k is the von Kármán constant, 0.41. Broken line is Dean's wake function; +denotes values of Dean's wake strength parameter, $\Pi = 0.5, 0.3, 0.1, 0, -0.1$. Tagged symbols are for low Reynolds numbers, $1590 < U_e\theta/\nu < 2000$.

approximately compensating effects of change in $(u'/U)_e$ and L_e^u/δ_{995}. Set E, for example, shows no such apparent self-preservation.

It was demonstrated in I that the dependence of the skin friction on both intensity and lengthscale could be correlated in terms of a single parameter, $\beta \equiv (u'/U)_e/(L_e^u/\delta_{995}+2)$. Lines of β = constant are shown in figure 2. Although this parameter was originally devised empirically from the change of skin friction at constant momentum-thickness Reynolds number, $U_e\theta/\nu$, it is equally useful for correlating the change at constant displacement-thickness number, $U_e\sigma^*/\nu$, and the change in the wake strength (the deviation from the logarithmic law) and other integral parameters, such as δ^*/θ. Any strict inconsistency between these as 'universal' correlations is no larger than the range of the scatter in the present data, which is comparable for each correlation. Since, in general, the velocity defect, $(U_e-U)/u_\tau$, where u_τ is the friction velocity, will formally depend upon both $(u'/U)_e$ and L_e^u/δ_{995}, a wake function with a single wake-strength argument would strictly be inadequate. However, Figure 4 indicates no strong separate dependence on these two parameters. Figure 3 also shows the wake function of Dean (see I) for all profiles except one (set H), for which a value of the wake strength parameter, Π, does not exist. This wake function is better suited to the present data than, say, that of Coles (1956), but can only simultaneously satisfy the wall shear stress and the displacement thickness if $\Pi > -\frac{5}{12}$ is implied. Curiously, Dean's wake function improves from a moderately good fit to a very good fit before it fails for the very 'full', long-tailed velocity profiles that occur in high free-stream turbulence. Castro (1984) gives a basis for a modification to the mean-flow correlations with β for boundary layers at low Reynolds numbers ($U_e\theta/\nu \lesssim 2000$).

3.2. *Conventionally averaged measurements*

3.2.1. *Reynolds stresses*

Figure 5 shows Reynolds direct- and shear-stress profiles normalized by u_τ^2 for $(u'/U)_e = 0, 0.025, 0.040$, and 0.058. With the apparent exception of case H, the edge

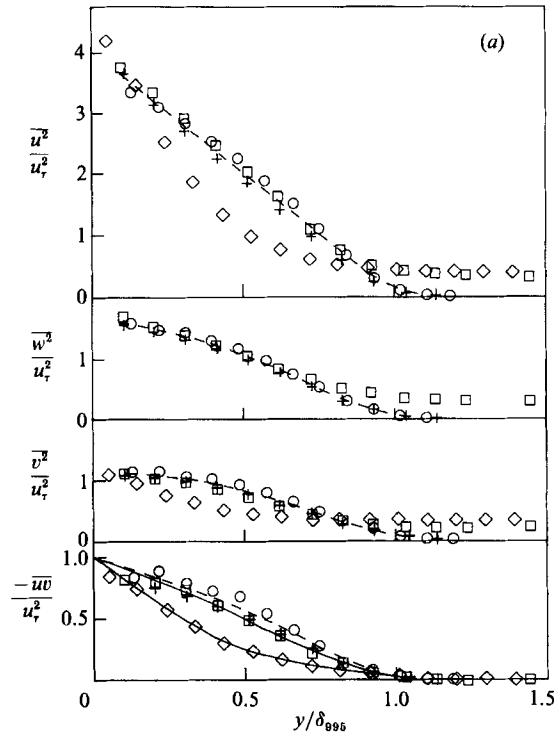

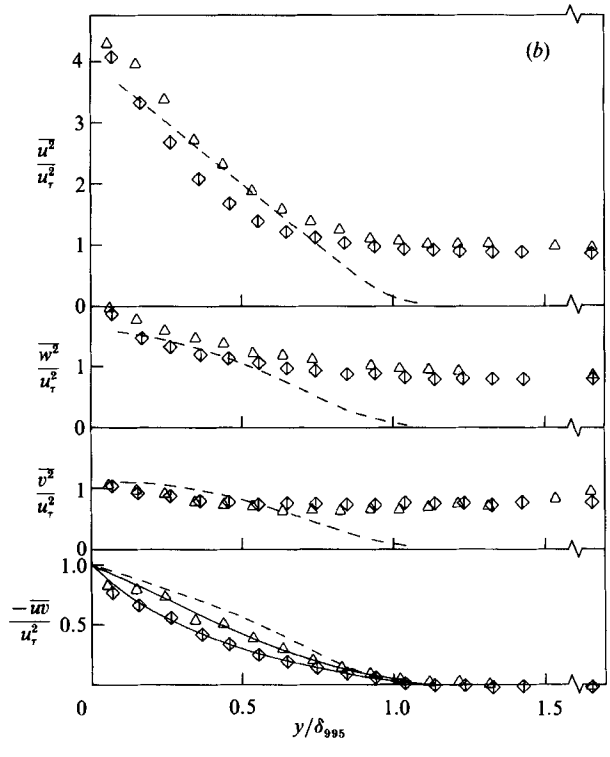

FIGURE 5(*a*,*b*). For caption see facing page.

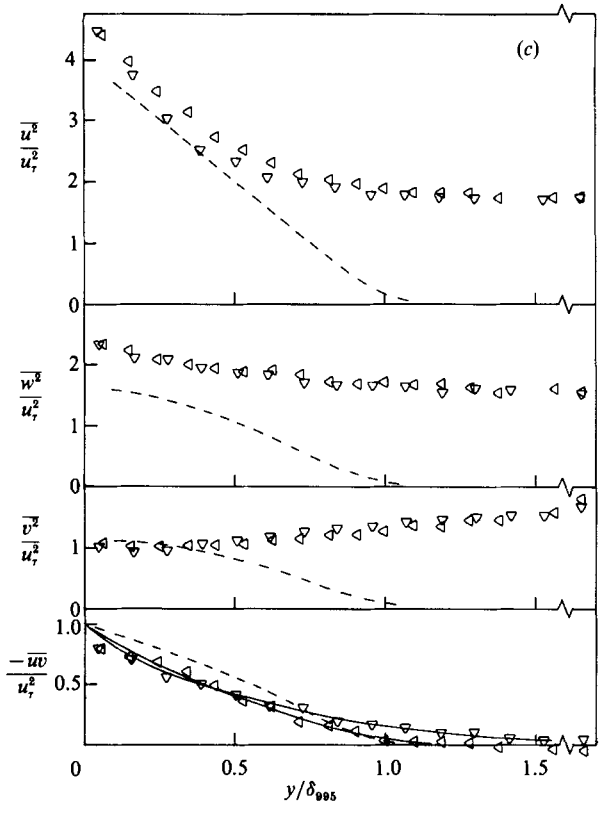

FIGURE 5. Reynolds stresses. Note different scale for $-\overline{uv}$. Symbols correspond to those given in table 1, and the broken lines are faired curves through data for $u_e' = 0$, indicated by ○ and + on (*a*). (*a*) $(u'/U)_e = 0$ and ≈ 0.025, $L_e^u/\delta_{995} = 1.88$ (□); $= 0.67$ (◇). (*b*) $(u'/U)_e \approx 0.040$, $L_e^u/\delta_{955} = 1.90$ (△); $= 0.71$ (◈). (*c*) $(u'/U)_e \approx 0.058$, $L_e^u/\delta_{995} = 1.83$ (◁); $= 1.34$ (▽).

of the shear stress profile, δ_{05}, defined as the position at which $-\overline{uv} = 0.05u_\tau^2$, is only slightly affected in relation to the mean velocity profile edge, δ_{995}, and is dependent more on length-scale than on intensity. For case H, δ_{995} is also inconsistent with other measurements, such as that of intermittency: the likely explanation is the low accuracy of δ_{995} arising from the very low velocity gradient $\partial U/\partial y$ (figure 3). Tentatively, δ_{995} should perhaps be roughly a factor 1.4 larger for this one case, but we have made no adjustment to the data.

Two immediately noticeable features in figure 5 are that, compared with the case when free-stream turbulence is absent, the direct stresses are not always increased, contrary to what might be expected, and that the shear-stress profiles are always more concave upwards, the effect being more marked at the lower L_e^u/δ_{995}†. The first feature is particularly evident at the lower lengthscale in figure 5(*a*), where $\overline{u^2}$ and $\overline{v^2}$ (and presumably $\overline{w^2}$, which was not measured for this case) are considerably reduced over a substantial part of the outer layer. Both features are most likely due in part to reduced production and generation arising from the reduced mean velocity

† Although this change in shape does not correlate with β this does not contradict the good correlation of wake strength with β, because correlation of shear-stress profiles (and intensity profiles) would require the conditions for self-preservation to be met, namely $(\delta/u_\tau)(\mathrm{d}u_\tau/\mathrm{d}x) \propto \mathrm{d}\delta/\mathrm{d}x$ and $u_\tau \propto U_e$, which they are not.

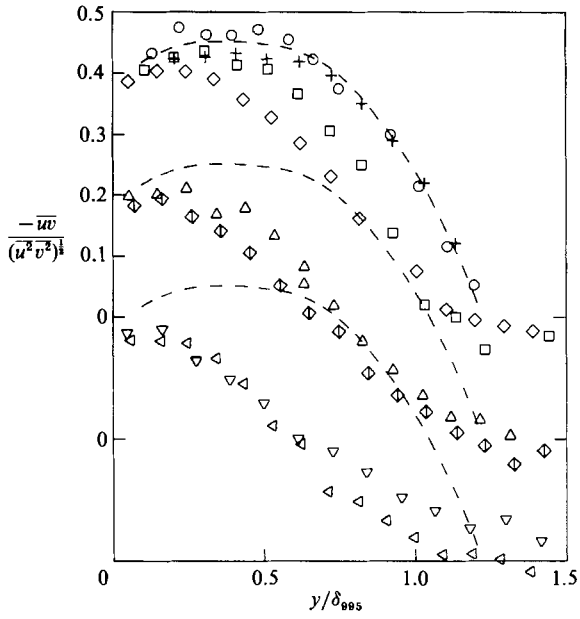

FIGURE 6. Shear-stress correlation coefficient. $(u'/U)_e$ and L_e^u/δ_{995} as defined by corresponding symbols in table 1. Broken line is through data for $u_e' = 0$.

gradient $\partial U/\partial y$. As might be expected, $\overline{v^2}$ remains proportional to u_τ^2 in the inner layer, independent of free-stream intensity or lengthscale.

A further noticeable feature in some cases, particularly in figure 5(*c*), is a decrease in v-component intensity from the free-stream value proper before the expected rise in the boundary-layer region. The reason for this decrease is the normal-component velocity constraint $v = 0$ at the surface, whose effect was demonstrated experimentally by Thomas & Hancock (1977) and theoretically by Hunt & Graham (1978). Briefly, the v-component intensity is attenuated by the surface constraint at distances from the surfaces less than about L_e^u: nominally, both the u- and w-components are increased in the same region, but in the experiments of Thomas & Hancock the increase in the w-component was considerably less than that in the u-component. Of course, near the surface u and w are dominated by the tangential velocity viscous constraint, $u = w = =0$, at the surface, as demonstrated at low Reynolds numbers by Uzkan & Reynolds (1967) from measurements of u. (The reduction in v would be more evident from low-wavenumber spectra of v, but no detailed spectral analysis was made.) As a consequence of this 'wall effect' the free stream in this paper is defined as the region beyond which the intensities cease to vary with y, and not as the region just beyond the boundary layer mean velocity edge, say.

Figure 6 shows the shear correlation coefficient $\overline{uv}/(\overline{u^2}\overline{v^2})^{\frac{1}{2}}$. (The shear-stress/intensity ratio $-\overline{uv}/\overline{q^2}$ behaves in a similar manner to the correlation coefficient and so is not included here, $\overline{q^2} = \overline{u^2} + \overline{v^2} + \overline{w^2}$.) As observed by previous workers (but see the discussion in I), the main effect of free-stream turbulence is to decrease the parameter in the outer part of the boundary layer, where the shear stress must go to zero but the intensity does not. The decrease is larger at the lower lengthscale. The aforementioned reduction in v-component free-stream intensity near the wall implies that the effect of a turbulent free stream on the inner layer, $y/\delta \lesssim 0.2$, say, will be

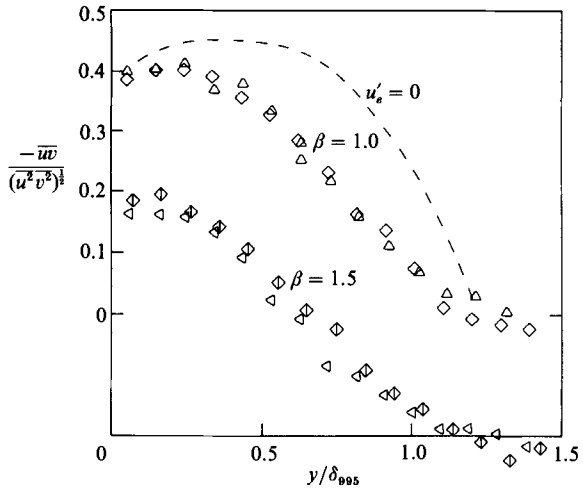

FIGURE 7. Shear-stress correlation coefficient at constant β. Symbols as in table 1.

largely to increase the u-component and w-component fluctuations by the addition of 'inactive' motion parallel to the surface, which does not contribute to the shear stress $-\overline{\rho uv}$. Thus, the apparent weak dependence on L_e^u/δ_{995} in the inner layer is probably due to increased 'inactive' motion at higher L_e^u/δ_{995} tending to cancel the lengthscale dependence in the outer layer. The shear-correlation-coefficient profiles correlate well with β for the two values ($\beta = 1$ and 1.5) at which comparison can be made, as shown in figure 7. However, whilst the shear stress is constrained by the conservation of mean momentum the turbulent kinetic energy and other quantities are not, and so we regard correlations of turbulence quantities with β as noteworthy but nevertheless empirical observations.

3.2.2. *Triple velocity products*

Some triple products are given with the conditionally sampled measurements in the next section and in detail by Hancock (1980), but for the present are summarized by the behaviour of the 'transport velocities' $V_\tau = \overline{uv^2}/\overline{uv}$ and $V_q = \overline{q^2 v}/\overline{q^2}$, shown in figure 8. Both V_τ and V_q are increased substantially inside $y \approx 0.5\delta_{995}$ and decreased substantially outside this position, V_q reaching zero just outside δ_{995} essentially because $\overline{q^2 v}$ tends to zero there while $\overline{q^2}$ does not, of course. The departure of V_τ and V_q in the outer layer from those when $u'_e = 0$ is noticeably greatest in each case for the smaller free-stream lengthscale. V_τ and V_q correlate fairly well with β, although the limited amount of data also exhibits a comparably good correlation of V_τ with L_e^u/δ_{995}.

3.3 *Conditionally sampled measurements*

3.3.1. *Intermittency*

For a more detailed explanation of the effect of free-stream turbulence on the boundary layer, we need to consider conditionally sampled turbulence statistics. Photographs of a smoke-filled boundary layer, at a rather low Reynolds number ($U_e\theta/\nu \approx 700$) are shown in figure 9. As expected, the effect of free-stream turbulence is to increase the irregularity of the boundary between the boundary-layer fluid and the external-stream fluid. Quantitatively, this is best expressed in terms of the

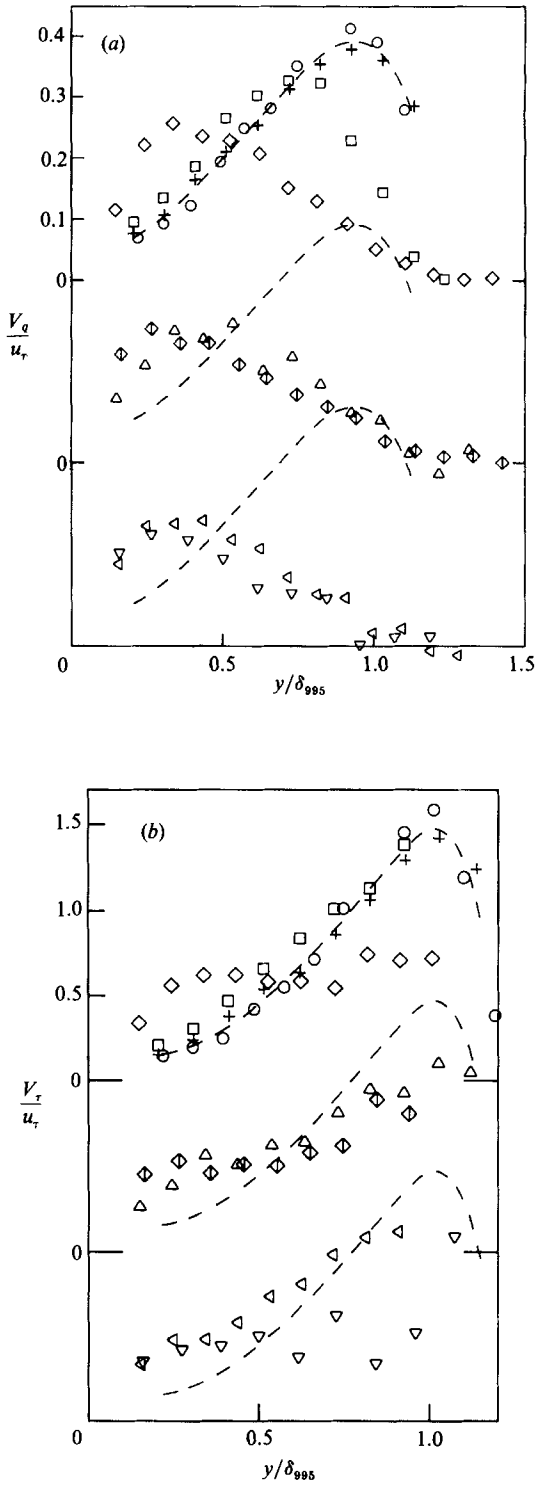

FIGURE 8. Turbulent transport velocities. $(u'/U)_e$ and L_e^u/δ_{995} as defined by symbols in table 1. Broken line is through data for $u'_e = 0$. (*a*) Turbulent shear-stress transport velocity, V_q. (*b*) Turbulent shear-stress transport velocity, V_r.

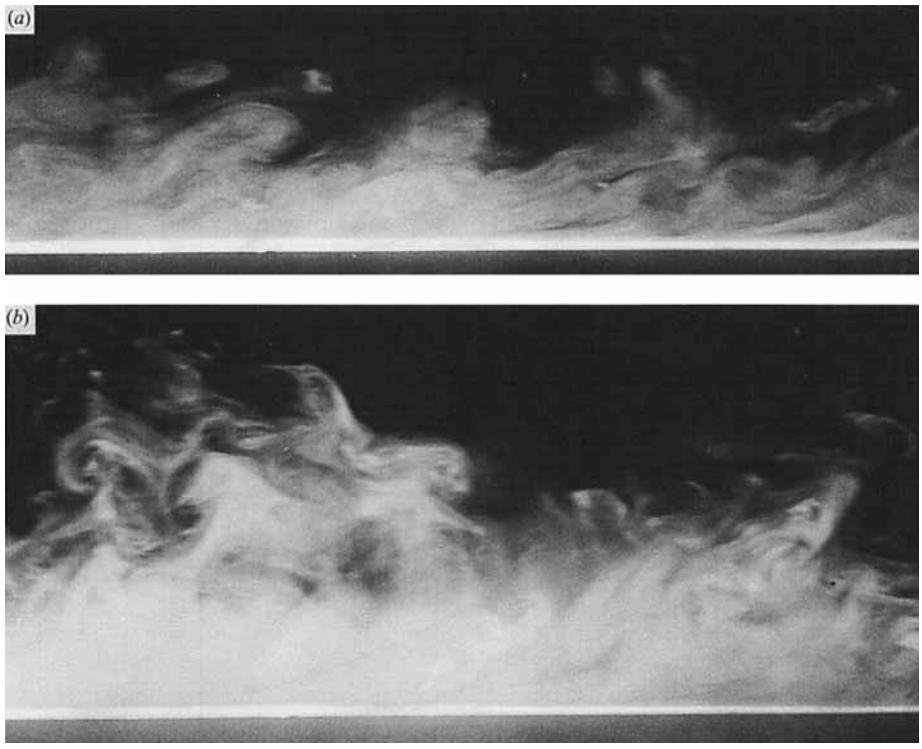

FIGURE 9. Transverse view of a turbulent boundary layer illuminated by thin vertical plane of light. (*a*) $(u'/U)_e \approx 0$. (*b*) $(u'/U)_e \approx 0.03$, $L_e^u/\delta_{995} \approx 0.4$. Flow is left to right.

behaviour of the intermittency factor γ, defined as the fraction of total time for which the flow at the measured position is 'hot', and of the 'burst frequency', f_γ, defined as the average number of 'hot' intervals per unit time. Figure 10 shows the intermittency profiles at two stations along the plate for the case $u'_e = 0$, together with profiles measured by other workers. The intermittency measurement method of Andreopoulos & Bradshaw (1980) was essentially the same as the present method, whilst Klebanoff (1955), Kovasznay, Kibens & Blackwelder (1970), and Hedley & Keffer (1974*a*) employed velocity-discrimination techniques.

From figure 10 it can be seen that the general effect of free-stream turbulence is to increase the standard deviation of the intermittency profile, consistent with the effect of increased mixing in the outer part of the boundary layer, and to alter its mean, $\bar{y}$, (i.e. the position at which $\gamma = 0.5$) as a fraction of the boundary-layer thickness. The change in the mean position, though marked, is also limited and so δ_{995} remains a relevant, if less precise, scale of the outer layer eddies of the boundary-layer fluid. Surprisingly, for the greater part of the intermittent region the effect of an *increase* in free-stream lengthscale leads to a *decrease* in γ, despite the fact that the effect on the mean flow is less. Presumably, this occurs because a large free-stream eddy is able to sweep further into the boundary layer, thereby increasing the amount of 'cold' fluid. The effect on the intermittency profile cannot be accounted for simplistically in terms of a smaller v at the larger L_e^u/δ_{995} leading to a smaller rate of transport and, hence, a smaller effect at the larger lengthscale; in any case the reduction in v is small outside $y \approx \bar{y}$ for the present L_e^u/δ_{995}. However, the wall effect

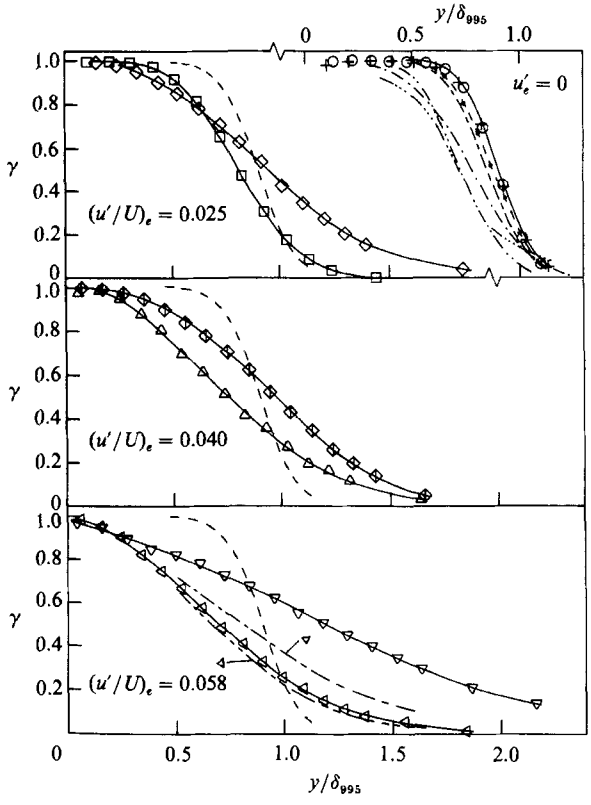

FIGURE 10. Intermittency factor. $(u'/U)_e$ and L^u_e/δ_{995} as defined in table 1. Broken line is through data for $u'_e = 0$. Top right of figure includes measurements of other workers: —•—, Andreopoulos & Bradshaw (1980); – – –, Klebanoff (1955); – · –, Charnay *et al.* (1976); – · · –, Kovasznay *et al.* (1970); –...–, Hedley & Keffer (1974*a*) Bottom part of figure also shows γ *vs.* y/δ_{05} for cases G and H, as identified by symbols.

would dominate at a very large lengthscale and γ would have again to return to that when $u'_e = 0$ if the response of the boundary layer were to tend to a quasi-steady one of long-wavelength oscillation in the free-stream speed. At the lowest intensity the interaction is evidently weak at the larger lengthscale in that the intermittency and other turbulence and mean-flow quantities do not differ greatly from those when $u'_e = 0$. This suggest, as might be expected, that the intensity at which the interaction may be regarded as weak increases with lengthscale. A further notable feature is that the edge of the intermittency profile, defined by the point at which (say) $\gamma = 0.05$ tends to a constant proportion of δ_{05}, independent of free-stream intensity or lengthscale. Values of $\bar{y}$ and a measure of the standard deviation, σ, defined by $\sigma^{-1} = (2\pi)^{\frac{1}{2}}(\mathrm{d}\gamma/\mathrm{d}y)_{y=\bar{y}}$, are included in table 1.

Figure 11 shows the 'burst frequency', which is strongly dependent on the definition of a 'burst' and upon the ability of the 'hot/cold' discrimination technique to identify short 'cold' intervals in the middle of a burst: one such interval clearly doubles the burst frequency. The maximum dimensionless frequency obtained in the present experiments in the absence of the turbulence grid is in the same range as that measured by previous workers (references in figure 10). Generally, the typical burst frequency is increased by free-stream turbulence, corresponding to the increased raggedness of the smoke interface shown in flow-visualization experiments,

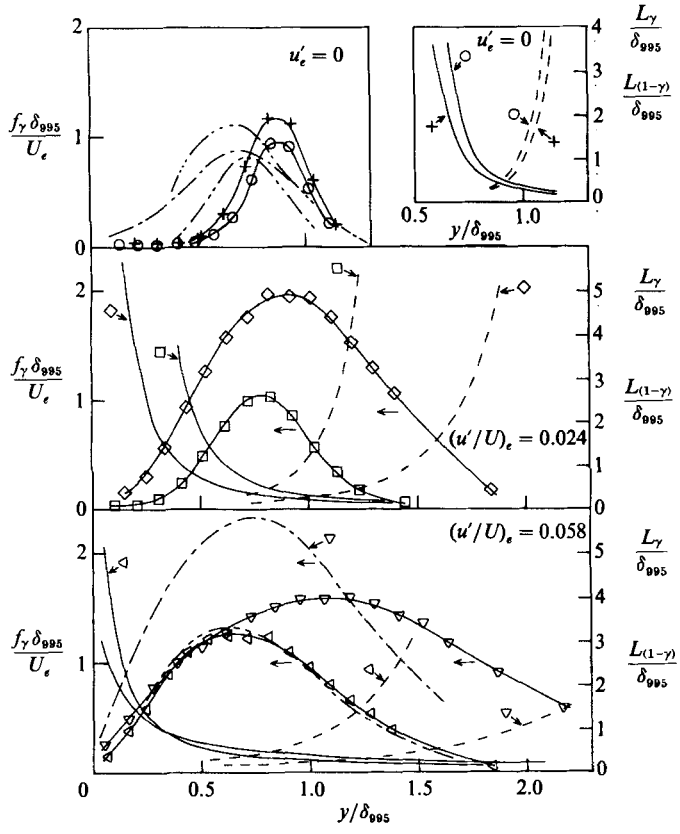

FIGURE 11. Burst frequency and average lengths of hot and cold bursts. Symbols as in table 1. ——, L_γ; --- $L_{(1-\gamma)}$): cases identified by symbols. Bottom part of figure also shows $f_\gamma \delta_{05}/U_e$ *vs.* y/δ_{05}, for cases G and H, as identified by symbols.

while the frequency tends to decrease as the free-stream turbulence lengthscale increases, consistent with the above inference of greater penetration of larger free-stream eddies. In fact, the peak frequency is roughly proportional to U_e/L_e, but differs rather spectacularly in maximum value and in distribution from the results for a non-turbulent free stream. Figure 11 also shows the average lengths of the hot and cold bursts based on γ, f_γ and the local conventionally averaged mean velocity, namely $L_\gamma = \gamma U(y)/f_\gamma$ and $L_{(1-\gamma)} = (1-\gamma)\, U(y)/f_\gamma$. The intermittency factor and burst frequency do not correlate with β.

The intermittency measurements of Charnay *et al.* (1976) show rather smaller variation of mean and standard deviation with increasing turbulence intensity than do the present results, even allowing for the smaller range of lengthscale in Charnay *et al.*'s experiment. Charnay *et al.*'s no-grid burst frequency results are implausibly *high* near the surface, where the burst frequency should go to zero as the intermittency factor goes to unity. This is possibly a consequence of the poorer frequency response of his temperature-measurement circuit. Nevertheless, in the outer layer the maximum is broadly comparable with our results, as is the increase in the maximum when free-stream turbulence is present.

As in previous papers in this series, conditionally sampled results are presented in terms of excursions from the conventional-average velocity, rather than using zone-average velocities as the base line for velocity fluctuations in the 'hot' and 'cold'

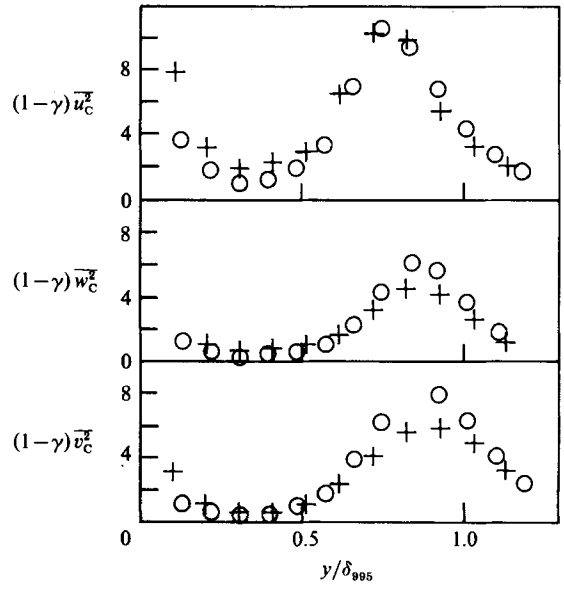

FIGURE 12. Cold-zone contributions to $\overline{u^2}$, $\overline{w^2}$, and $\overline{v^2}$ in the absence of free-stream turbulence. Symbols as in table 1. All quantities normalized by $U_e^2 \times 10^{-5}$.

zones. An average quantity Q (say a mean-square intensity) evaluated with respect to the conventional-average velocity obeys $Q = \gamma Q_H + (1-\gamma) Q_C$, where Q_H and Q_C are the hot and cold zone averages, and γQ_H and $(1-\gamma)Q_C$ can conveniently be called the zonal contributions to Q. For further discussion see Dean & Bradshaw (1976). Charnay *et al.* measured velocity excursions from the zone-averaged velocities, but this has the drawback of ignoring the main contribution from the large-scale motion to the conventionally averaged turbulence quantities.

3.3.2. *Reynolds stresses*

In the absence of free-stream turbulence, the 'cold' (i.e. irrotational)-zone contributions to the mean-square intensities reach maxima in the outer part of the boundary layer, as shown in figure 12, but are small compared with the hot (i.e. turbulent)-zone contributions, which differ little, therefore, from the conventionally averaged intensities. The rise in the cold-zone contributions near the wall is probably because of the failure of the intermittency algorithm to fully discriminate short, infrequent cold zones. The addition of free-stream turbulence implies, of course, that the cold-zone contributions asymptote to the free-stream turbulence level, while the 'hot' contributions fall to zero at the outer edge of the boundary layer as usual. Figure 13 shows the zonal contributions to $\overline{u^2}$, $\overline{w^2}$, $\overline{v^2}$ and $-\overline{uv}$ for two typical cases. Figure 13 also shows profiles of $(1-\gamma)\overline{u_e^2}$ and $(1-\gamma)\overline{w_e^2}$, which are the contributions that would exist if the cold zone was simply filled with unaltered free-stream turbulence. $(1-\gamma)\overline{u_C^2}$ is substantially larger than $(1-\gamma)\overline{u_e^2}$, at the larger lengthscale, and distinguishably larger at the smaller lengthscale, while $(1-\gamma)\overline{w_C^2}$ and $(1-\gamma)\overline{w_e^2}$ are very close. The turbulence in the cold zone can be expected to differ from that which would exist in the absence of the boundary-layer turbulence because of the mean and fluctuation motion caused by the hot-zone turbulence. The increase of the u-component and w-component cold-zone intensities with distance from the surface

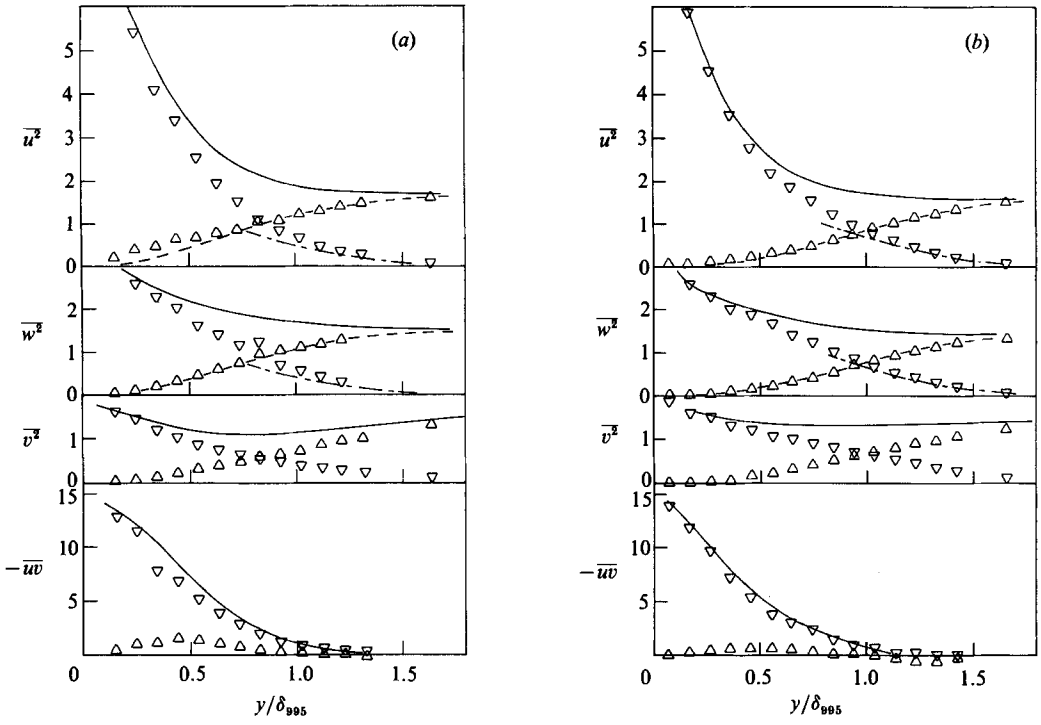

FIGURE 13. Zonal contributions to $\overline{u^2}$, $\overline{w^2}$, $\overline{v^2}$ and $-\overline{uv}$ for (*a*) $(u'/U)_e = 0.041$, $L_e^u/\delta_{995} = 1.90$ (case C3); (*b*) $(u'/U)_e = 0.040$, $L_e^u/\delta_{995} = 0.71$ (case E1). ∇, hot-zone contributions $\gamma\overline{u^2_{\rm H}}$, $\gamma\overline{w^2_{\rm H}}$, $\gamma\overline{v^2_{\rm H}}$ and $-\gamma\overline{uv}_{\rm H}$. $\triangle$, cold-zone contributions $(1-\gamma)\overline{u^2_{\rm C}}$, $(1-\gamma)\overline{w^2_{\rm C}}$, $(1-\gamma)\overline{v^2_{\rm C}}$ and $-(1-\gamma)\overline{uv}_{\rm C}$. ——, conventionally averaged quantities. All quantities normalized by $U_e^2 \times 10^{-3}$. – – –, $\gamma\overline{u^2}_e$ and $\gamma\overline{w^2}_e$; – – –, $(1-\gamma)\overline{u^2}_e$ and $(1-\gamma)\overline{w^2}_e$. Note different scale for the shear stress.

is distinctly more rapid than for the v-component at the larger lengthscale, consistent with the attentuation of the latter by the normal-component velocity constraint at the surface. The fact that $\gamma\overline{w^2_{\rm C}}$ is closely equal to $\gamma\overline{w^2_e}$ and that there is no mean W motion suggests that the fluctuating motion caused by hot-zone fluid remains small, consistent with the comparatively much smaller change in the hot-zone Reynolds stresses with the addition of free-stream turbulence. Consequently, the large cold-zone contribution to $\overline{u^2}$ is likely to be due mainly to interaction with the mean U motion in the cold zone caused by the hot-zone turbulence. The cold-zone measurements by Charnay *et al.* are dubious in that the v-component rises towards the surface.

The cold-zone contribution to the shear stress $-\rho\overline{uv}$ shown in figure 13 is small but not negligible inside $y = \delta_{995}$ and negligible outside this position. Clearly, the shear stress in the substantial quantity of hot fluid outside $y = \delta_{995}$ is also negligible. Inside $y = \delta_{995}$ the hot-zone shear correlation coefficient shown, in figure 14, decreases with increasing intensity, and, at constant intensity, it also decreases with decreasing free-stream lengthscale. That is, the structure is less affected at the higher lengthscale even though the incursions of cold fluid are deeper and longer. This lengthscale dependence together with the deeper incursions of cold fluid for large free-stream lengthscale is particularly interesting in that it suggests that the hot-zone structure is strongly dependent upon the fluctuating strain rates $\partial u/\partial x, \partial u/\partial y + \partial v/\partial x$, etc. imposed by the cold-zone motion; presumably, these strain rates are proportional to

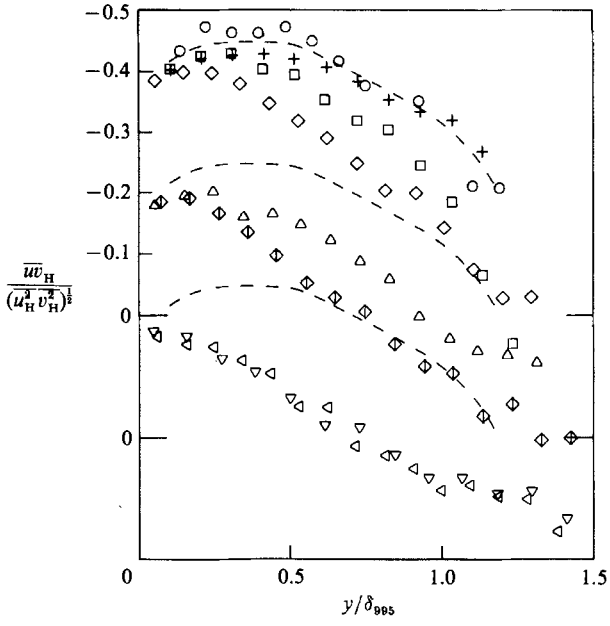

FIGURE 14. Hot-zone shear-stress correlation coefficient. Symbols as in table 1. Broken line is through data for $u'_e = 0$.

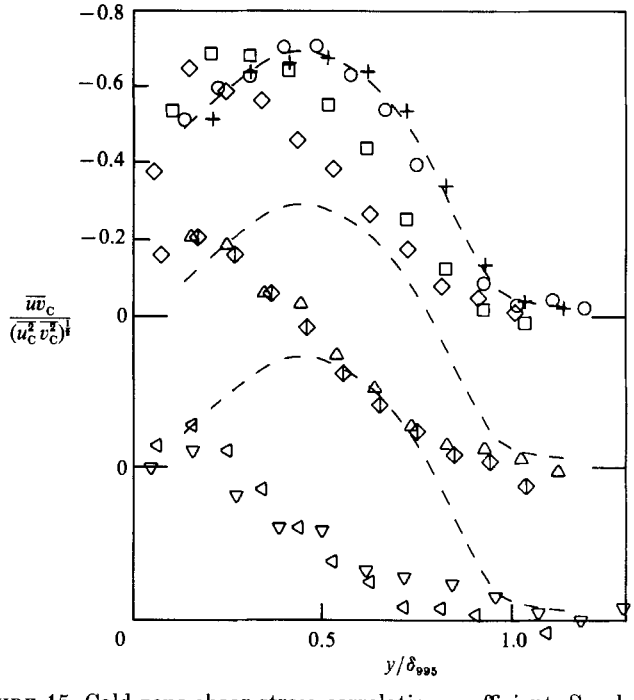

FIGURE 15. Cold-zone shear-stress correlation coefficient. Symbols as in table 1. Broken line is through data for $u'_e = 0$.

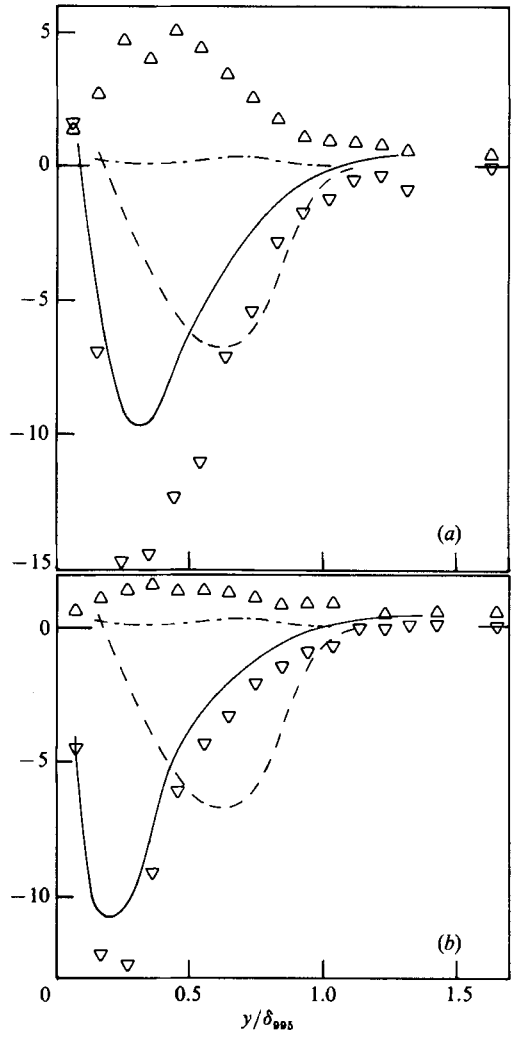

FIGURE 16. Zonal contributions to $\overline{u^3}$ for $(u'/U)_e \approx 0.040$. ∇, $\gamma\overline{u_H^3}$; $\triangle$, $(1-\gamma)\overline{u_C^3}$; ——, $\overline{u^3}$. – – –, –·– are, respectively, $\overline{u^3}$ and $(1-\gamma)\overline{u_C^3}$ for $u'_e = 0$. All quantities normalized by $U_e^3 \times 10^{-5}$. (*a*) $L_e^u/\delta_{995} = 1.90$. (*b*) $L_e^u/\delta_{995} = 0.71$.

the cold-zone intensity and inversely proportional to the size of the intruding eddies. For sufficiently large lengthscale they would be negligible compared with those in the shear layer proper.

Interestingly, the cold-zone shear correlation coefficient, shown in figure 15, reaches values of about -0.7 in the middle part of the boundary layer, in the absence of free-stream turbulence, indicating that a large u-component velocity in the cold zone is usually associated with an inward v-component motion, and vice versa. A similarly large correlation coefficient can be deduced from measurements of Headley & Keffer (1974*b*) and Charnay *et al.* after referring the external fluctuations to the conventional rather than the conditional mean velocity. The behaviour or the turbulent bursts and the irrotational motion in the outer part of the turbulent boundary layer seem to be rather similar to the 'burst and sweep' mechanism identified by many workers in the inner part of the boundary layer (Brown &

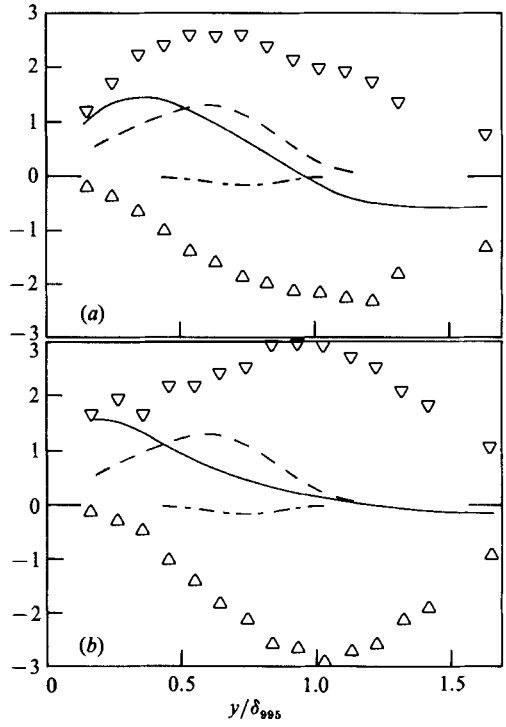

FIGURE 17. Zonal contributions to $\overline{v^3}$ ▽, $\gamma\overline{v_H^3}$; △, $(1-\gamma)\,\overline{v_C^3}$; ——, $\overline{v^3}$. – – –, – · –, are, respectively, $\overline{v^3}$ and $(1-\gamma)\overline{v_C^3}$ for $u_e' = 0$. Other details as figure 16.

Thomas 1977). Free-stream turbulence also decreases the cold-zone coefficient but in this case there appears to be no more than a weak lengthscale effect except at the lowest free-stream intensity. $-\overline{uv}_H/\overline{q_H^2}$ and $-\overline{uv}_C/\overline{q_C^2}$ behave very similarly to the respective correlation coefficient, and so are not included here. The zonal shear-stress correlation coefficients also correlate well with β.

3.3.3. *Triple products*

Figures 16–19 show the zonal contributions to the triple products $\overline{u^3}$, $\overline{v^3}$, $\overline{u^2v}$, and $\overline{uv^2}$ for $(u'/U)_e = 0.04$. In the absence of free-stream turbulence, the cold-zone contributions to these quantities are, in fact, very much smaller than the hot-zone contributions. This is to be expected if the probability distribution of the cold-zone fluctuations is not to be very highly skewed, because the cold-zone Reynolds-stress contributions are also small compared with the hot-zone contributions.

Free-stream turbulence increases both the hot- and cold-zone contributions to $\overline{u^3}$, the increase in the latter being large and roughly proportional to $(1-\gamma)(\overline{u_C^3})^{\frac{3}{2}}$. Furthermore, the cold-zone contributions seem to be significantly larger (figure 16) – though not so marked at the other $(u'/U)_e$ – for larger free-stream lengthscales, consistent with larger, more penetrating, ingoing cold-zone 'sweeps'.

The conditionally averaged measurements of $\overline{v^3}$, shown in figure 17, again generally indicate a cold-zone contribution opposite in sign to that of the hot-zone contribution and the conventional average. $(1-\gamma)\,\overline{v_C^3}$ is roughly proportional to $(1-\gamma)(\overline{v_C^2})^{\frac{3}{2}}$. An interesting feature is that both contributions are large well outside the boundary layer. The resultant negative conventional-average is probably

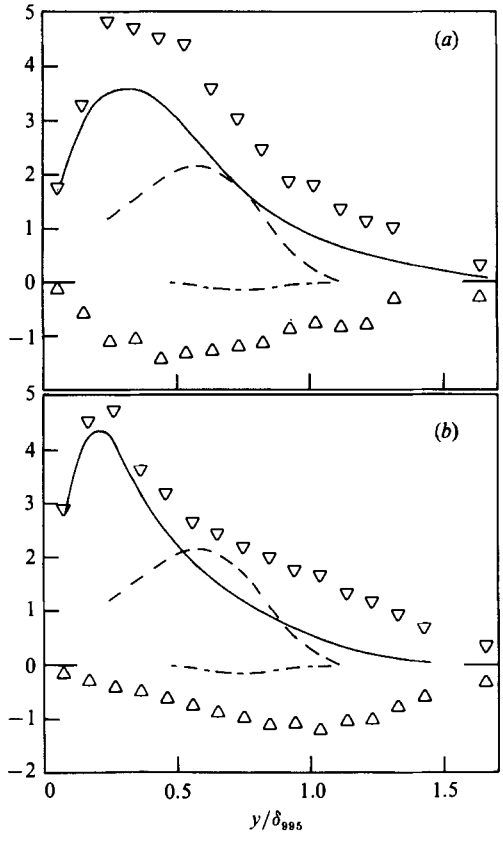

FIGURE 18. Zonal contributions to $\overline{u^2v}$. ▽, $\gamma\overline{u^2v}_{\mathrm{H}}$; △, $(1-\gamma)\overline{u^2v}_{\mathrm{C}}$; ——, $\overline{u^2v}$. – – –, – · – are, respectively, $\overline{u^2v}$ and $(1-\gamma)\overline{u^2v}_{\mathrm{C}}$ for $u'_e = 0$. Other details as in figure 16.

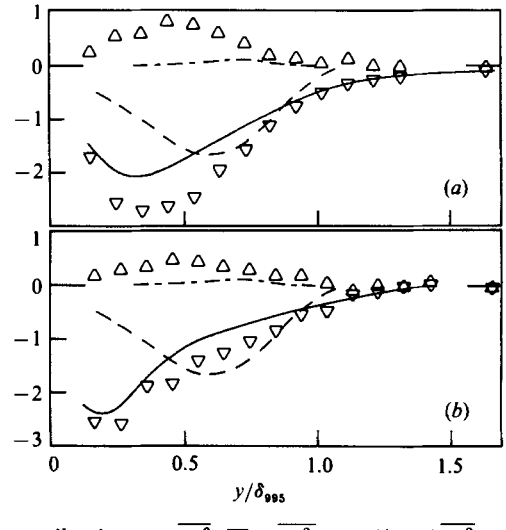

FIGURE 19. Zonal contributions to $\overline{uv^2}$. ▽, $\gamma\overline{uv^2}_{\mathrm{H}}$; △, $(1-\gamma)\overline{uv^2}_{\mathrm{C}}$; ——, $\overline{uv^2}$. – – –, – · – are, respectively, $\overline{uv^2}$ and $(1-\gamma)\overline{uv^2}_{\mathrm{C}}$ for $u'_e = 0$. Other details as in figure 16.

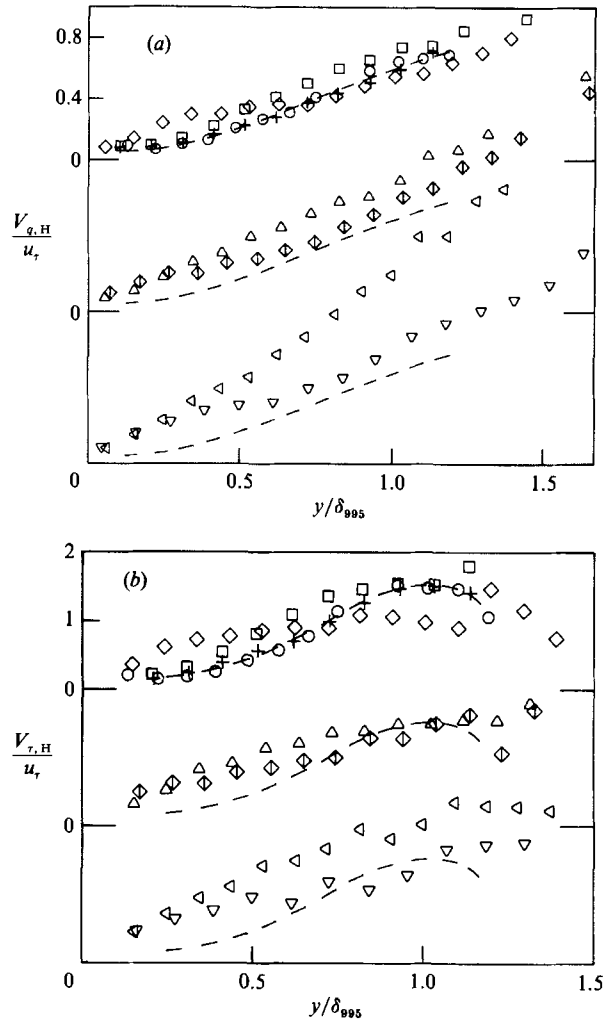

FIGURE 20. Hot-zone transport velocities. $(u'/U)_e$ and L_e^u/δ_{995} as defined by symbols in table 1. Broken line is through data for $u_e' = 0$. (*a*) Turbulent kinetic energy transport velocity $V_{q,H}/u_\tau$. (*b*) Shear-stress transport velocity $V_{\tau,H}/u_\tau$.

spurious in that it does not appear to tend to zero, though there is no obvious satisfactory explanation for such a level of error; pessimistically, the level shown should be regarded as indicative of the uncertainty in $\overline{v^3}$. Nevertheless, a region of negative $\overline{v^3}$ would imply diffusion of turbulent energy towards the wall, which is at least qualitatively reasonable in view of the decrease of the intensity of the normal-velocity component with decreasing distance from the surface as a result of the constraint at the surface. The zonal contributions to $\overline{u^2v}$ (figure 18) decrease more rapidly than those to $\overline{v^3}$, and the contributions to $\overline{uv^2}$ (figure 19) reach zero just outside δ_{995}.

Figures 20 and 21 show the hot- and cold-zone transport velocities of turbulent energy and shear stress which, as implied by the previous results, have opposite signs. The hot-zone shear-stress transport velocity, $V_{\tau,H} \equiv \overline{v^2}\overline{u}_H/\overline{uv}_H$, differs from the overall transport velocity V_τ, but not by a large amount, whereas the hot-zone kinetic-energy transport velocity, $V_{q,H} \equiv \overline{vq^2_H}/\overline{q^2_H}$ (which has been approximated by

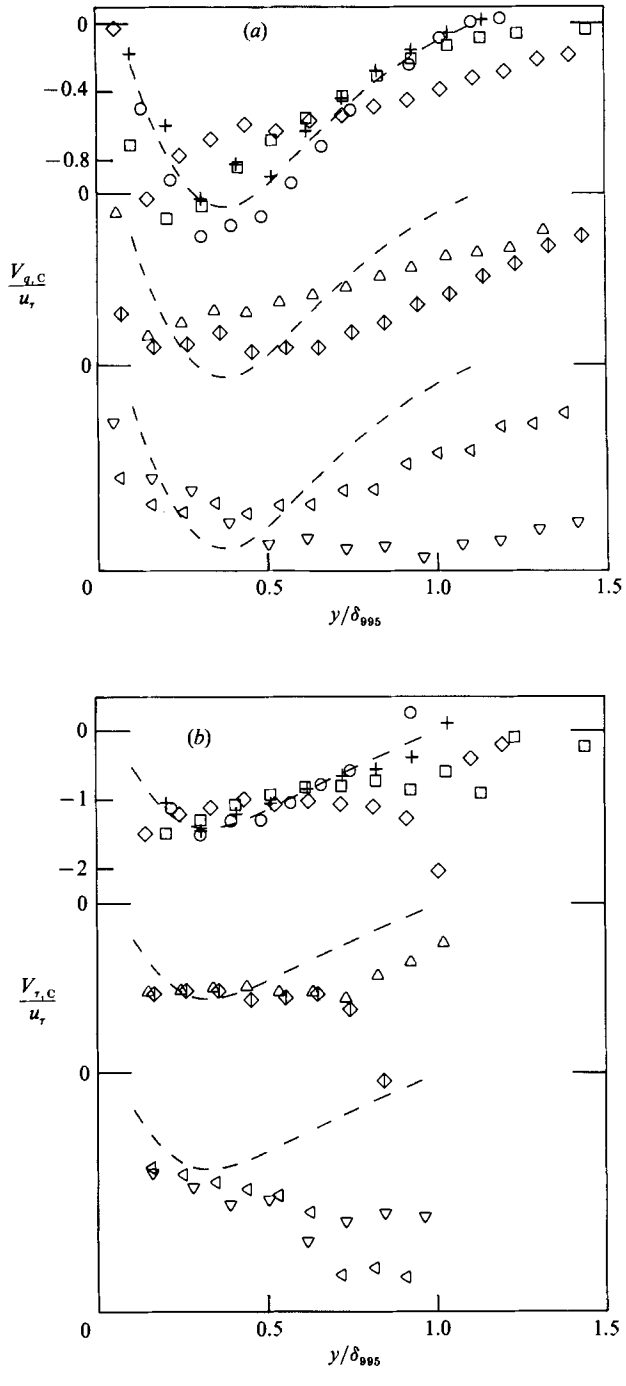

FIGURE 21. Cold-zone transport velocities. Symbols as in table 1. Broken line is through data for $u'_e = 0$. (*a*) Turbulent kinetic energy transport velocity $V_{q,C}/u_\tau$. (*b*) Shear-stress transport velocity $V_{\tau,C}/u_\tau$.

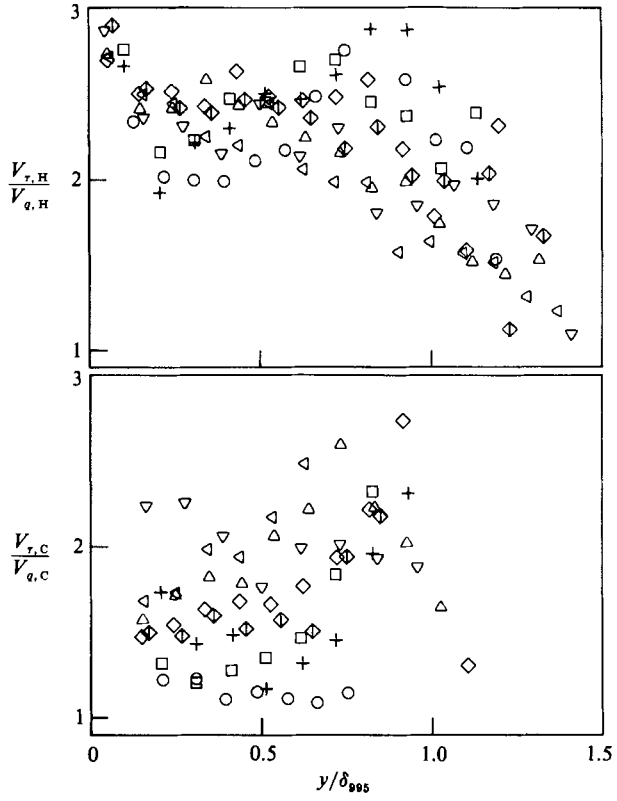

FIGURE 22. Ratio of hot-zone transport velocities, $V_{\tau,H}/V_{q,H}$, and ratio of cold-zone transport velocities, $V_{\tau C}/V_{q,H}$. Symbols as in table 1.

$\overline{v(u^2+v^2)}_H/(\overline{u_H^2}+\overline{v_H^2})$), differs substantially from V_q. $V_{\tau,H}$ and $V_{q,H}$ resemble those when free-stream turbulence is absent, though as a proportion they are increased substantially in the inner half of the layer. Even so, as shown in figure 22, $V_{\tau,H}/V_{q,H}$ is relatively unaffected, implying that the shear stress and turbulent energy are transported across the hot zone at the same relative rates. $V_{q,H}$ is particularly large well outside $y = \delta_{995}$ but, on the argument that there is no predominant transverse direction in the free stream, would eventually become zero. However, diffusion of temperature through entrainment would give a bias against inward-moving hot-zone fluid which on average must have been in the free stream for a longer time since it must have previously been outward-moving fluid. On the other hand, $V_{\tau,H}$ goes more readily to zero near the free stream presumably because there is no predominant u with either positive or negative v. $V_{\tau,C}/V_{q,C}$ (figure 22), where $V_{\tau,C} \equiv \overline{v^2}u_C/\overline{uv}_C$, and $V_{q,C}$ has been approximated by $\overline{v(u^2+v^2)}_C/(\overline{u_C^2}+\overline{v_C^2})$, is roughly constant. The scatter near $y = \delta_{995}$ is probably due to measurement and/or discrimination errors in $V_{\tau,C}$ where both denominator and numerator tend to zero.

3.4. *Fluctuating-strain rate*

Fluctuations in the cold zone impose fluctuations in the hot zone and hence fluctuating strains. In the previous section it was suggested that the hot-zone structure is principally affected by the fluctuating-strain rates imposed by the intruding cold-zone motions. The mean effect of these strain rates will scale upon the

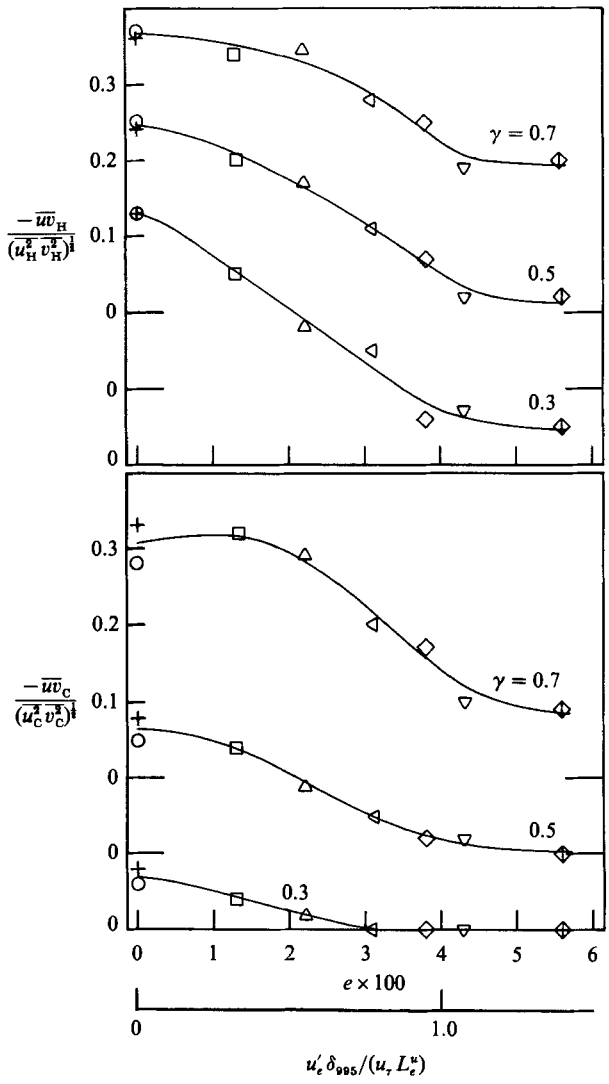

FIGURE 23. Variation of zonal correlation coefficients with the fluctuating-strain-rate parameter, e. Symbols as in table 1. Axis of $u'_e\delta_{995}/(u_\tau L_e^u)$ is shown for $u_\tau/U_e = 0.04$.

intensities and lengthscales of the cold-zone energy-containing motion, and in the simplest terms they will scale upon the intensity and lengthscale of the free-stream turbulence, i.e. upon u'_e/L_e^u. (More scales may be needed where the free-stream lengthscale is large enough for the wall-impermeability effect to be large in the outer layer.) Since the strain rate imposed by the mean motion will scale in simplest terms upon U_e/δ_{995} the relative fluctuating strain e, say, will be $(u'_e/L_e^u)/(U_e/\delta_{995})$, i.e. $e \equiv u'_e\delta_{995}/(U_e L_e^u)$. (More precisely, the mean velocity gradient scales on u_τ/δ_{995}, whereupon the parameter would be $u'_e\delta_{995}/(u_\tau L_e^u)$. However, compared with e, the variation in u_τ/U_e is comparatively small, and so we have employed the simpler definition of e.) Furthermore, because the interface position is affected, the effect of the fluctuating-strain rate on the hot-zone motion is more appropriately assessed at constant γ rather than constant y/δ_{995}. In the intensity–lengthscale plane lines of e = constant are straight lines of slope e^{-1} passing through the origin. Of course, since

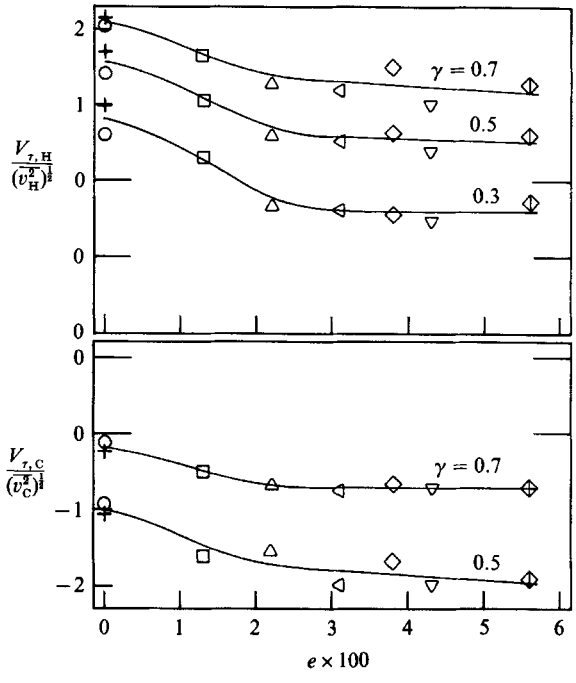

FIGURE 24. Variation of velocity ratios $V_{\tau,H}/(\overline{v_H^2})^{\frac{1}{2}}$ and $V_{\tau,C}/(\overline{v_C^2})^{\frac{1}{2}}$ with e.

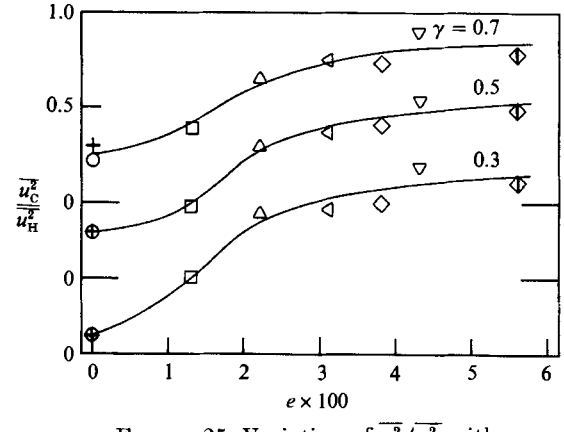

FIGURE 25. Variation of $\overline{u_C^2}/\overline{u_H^2}$ with e.

both u'_e/U_e and L^u_e/δ_{995} are independent parameters so too are any two combinations such as e and L^u_e/δ_{995}; the significance of e depends upon its success as a single parameter in correlating the change in structural parameters.

Corresponding arguments also apply to the cold-zone structure. A cold-zone eddy intruding into the boundary layer will be strained by the mean and fluctuating motion induced by the hot-zone fluid. The simplest measure of the mean-motion strain is U_e/δ_{995} and the simplest scales of an intruding eddy are u'_e and L^u_e, so that the non-dimensional mean strain will be $(U_e/\delta_{995})/(u'_e/L^u_e)$ – that is, e^{-1}. If the hot-zone structure is primarily dependent upon the fluctuating-strain-rate parameter, e, it follows that this parameter should also correlate the effect of the hot-zone fluctuating-strain rates imposed on the cold-zone motion.

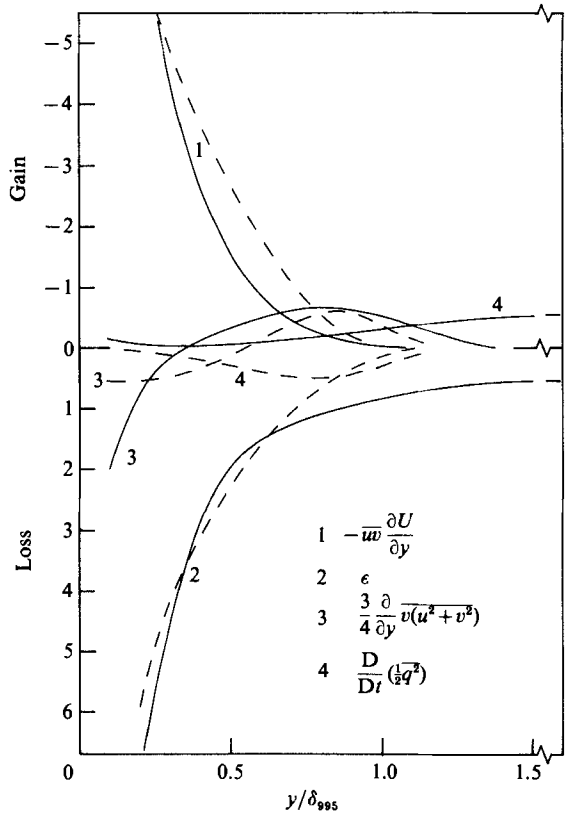

FIGURE 26. Balances of the turbulent-kinetic-energy transport equation. ——, $(u'/U)_e = 0.044$, $L_e^u/\delta_{995} = 2.23$. – – –, $u'_e = 0$ ($x = 2130$ mm). All quantities normalized by $\delta_{995} \times 10^4/U_e^3$.

Figures 23 and 24 show the variation with e of $-\overline{uv}_H/(\overline{u_H^2}\overline{v_H^2})^{\frac{1}{2}}$, $-\overline{uv}_C/(\overline{u_C^2}\overline{v_C^2})^{\frac{1}{2}}$ and $V_{\tau,H}/(\overline{v_H^2})^{\frac{1}{2}}$ for $\gamma = 0.3$, 0.5 and 0.7, and $V_{\tau,C}/(\overline{v_C^2})^{\frac{1}{2}}$ for $\gamma = 0.5$ and 0.7, the data at 0.3 being very scattered. Clearly, for each of these quatntities, there is a systematic dependence upon the strain-rate parameter. $-\overline{uv}_H/\overline{q_H^2}$, $-\overline{uv}_C/\overline{q_C^2}$, $V_{q,H}/(\overline{v_H^2})^{\frac{1}{2}}$ and $V_{q,C}/(\overline{v_C^2})^{\frac{1}{2}}$ exhibit comparable systematic variations with e, and so are not included. Not surprisingly, the hot-zone shear-stress contribution as a proportion of $(\overline{u_H^2}\,\overline{v_H^2})^{\frac{1}{2}}$ decreases more rapidly at lower γ. However, the tendency of the coefficients to become constant for large e is unexpected. Strikingly, the transport velocities tend fairly rapidly to become proportional to the hot-zone normal-component intensity, independent of e, implying a fairly rapid adjustment of the transport processes for kinetic energy and shear stress. The cold-zone correlation coefficients and transport velocities also become independent of e slightly more quickly than their hot-zone counterparts, it would appear.

The across-zone ratio $\overline{u_C^2}/\overline{u_H^2}$ (where the numerator and denominator are unweighted by $1-\gamma$ and γ) is shown in figure 25 for the same values of γ as above. This ratio also shows a systematic dependence upon e, as does $\overline{v_C^2}/\overline{v_H^2}$, which is not shown here, emphasizing the point that the motions in the hot and cold zones are linked via the fluctuating-strain-rate mechanism. A striking feature is that these ratios fairly quickly adjust with increasing e to roughly constant values, and that they are only weakly dependent upon γ

A larger vaue of δ_{995} for case H (giving, tentatively, $e = 0.06$) gives significantly less

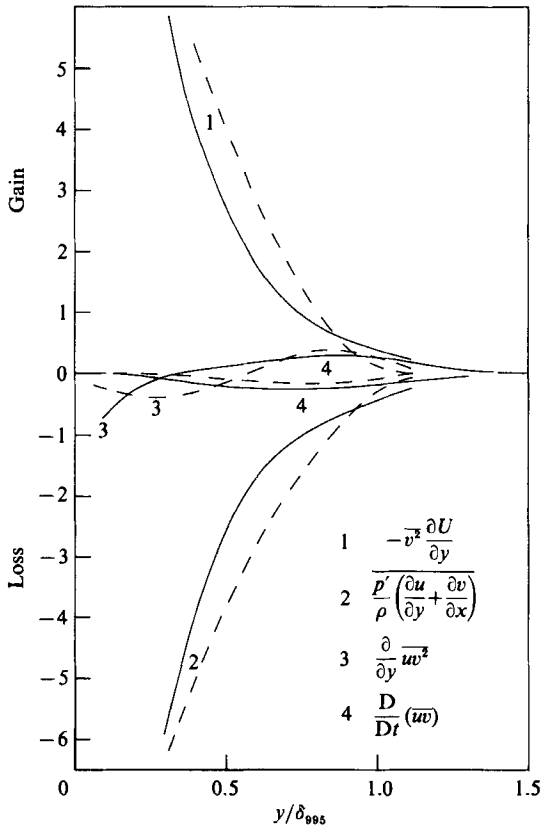

FIGURE 27. Balance of the turbulent shear-stress transport equation. Details as in figure 26.

scatter only for $\overline{u_C^2}/\overline{u_H^2}$ and $\overline{v_C^2}/\overline{v_H^2}$. Except, of course, where a structural parameter is constant, the above zonal parameters show no comparably good correlation with intensity or lengthscale, or, not unexpectedly, with the empirical parameter β. (Although β tends to e with increasing lengthscale, β and e are close only when the lengthscale is large – i.e. when both parameters are small – and the lengthscale is well beyond that for which the parameter β was established.)

3.5. *Transport-equation balances*

Figure 26 shows the terms in the turbulent kinetic-energy transport equation for boundary layers with and without free-stream turbulence. As expected, the introduction of free-stream turbulence implies non-zero dissipation in the free stream, balanced by advection. A non-obvious change is an increased loss of turbulent energy by diffusion from near the surface. Nevertheless, this rate of loss of turbulent energy is small compared with the production and dissipation, which implies that the local-equilibrium analysis leading to the logarithmic law is still valid. As usual, the shear-stress transport equation (figure 27) is more nearly in local equilibrium than the turbulent-energy equation, but again a pronounced loss by turbulent transport from the region near the wall is seen in the presence of free-stream turbulence. In all cases diffusion by pressure fluctuations has been neglected.

The dissipation rate and the pressure–strain correlation term were obtained, as usual, by difference of the other, measured, terms, and are therefore not of very high

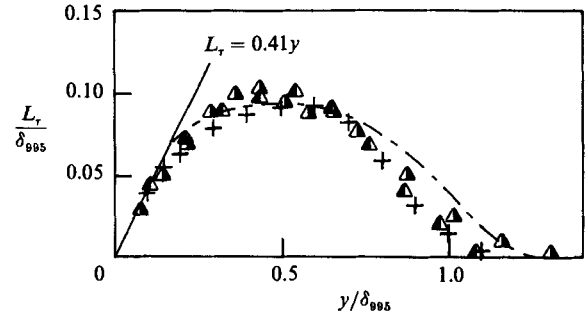

FIGURE 28. Dissipation lengthscale, L_r. Symbols defined in table 1. – – –, Bradshaw *et al.* (1967).

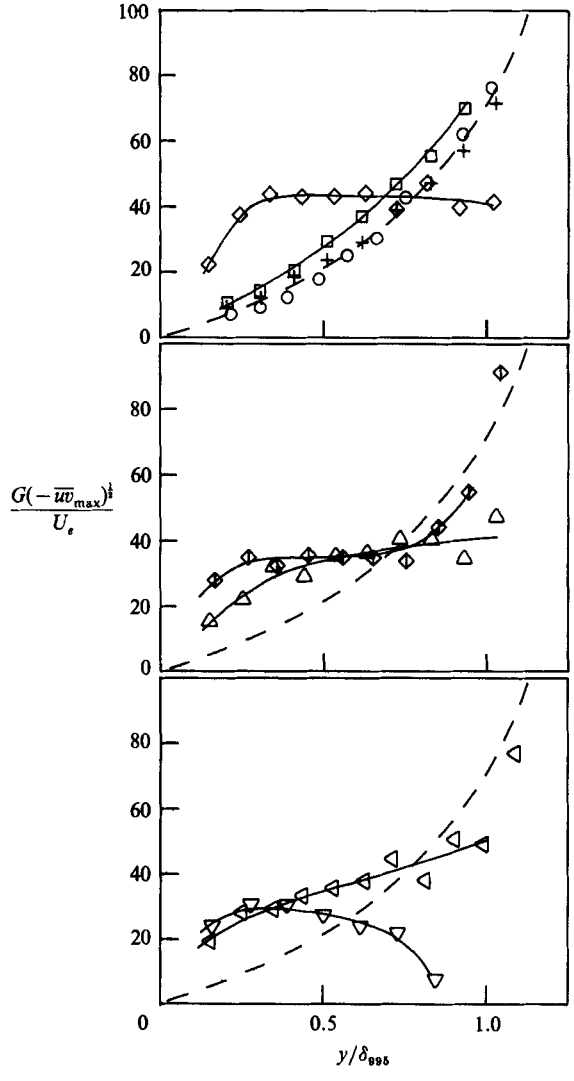

FIGURE 29. Diffusion function, G, factored by $(-\overline{uv}_{max})^{\frac{1}{2}}/U_e$. $(u'/U)_e$ and L_e^x/δ_{995} as defined in table 1. Broken line is through data for $u'_e = 0$.

accuracy. However, the values of the dissipation lengthscale $L_\tau = \tau^{\frac{3}{2}}/\epsilon$ deduced from the dissipation appear to be very little affected by free-stream turbulence (figure 28). This must be partly a coincidence, but does suggest that, over the main part of a boundary layer with free-stream turbulence, the shear stress provides a more meaningful velocity scale than does the turbulent kinetic energy: the lengthscale L_q based on the turbulent energy and the lengthscale varies considerably with free-stream turbulence intensity, as do the eddy viscosity and mixing length, which will not be discussed here. Figure 29 summarizes the triple-product results in terms of the diffusion function, G (approximated by $\frac{3}{4}\overline{v(u^2+v^2)}/(-\overline{uv}(-\overline{uv}_{\max})^{\frac{1}{2}})$) used in the calculation method of Bradshaw, Ferris & Atwell (1967) and this shows rather clearly the way in which free-stream turbulence increases the transport of turbulent energy near the surface, more so for the smaller lengthscale. The behaviour is not so clear in the outer part of the layer, where both $\overline{vq^2}$ and $\overline{uv}$ tend to zero near the boundary-layer edge, but the lengthscale dependence appears to be opposite to that in the inner part. G does not correlate well with β, and so the correlations of $\overline{uv}/\overline{q^2}$ or V_q/u_τ, or both, with β must at best be approximate.

4. Conclusions

Measurements of mean-flow parameters, and of conventionally and conditionally sampled turbulence quantities have been made in more detail and, in particular, over a wider range of free-stream lengthscale than previously. The significance of the latter parameter, which was found to be substantial, was expected for two reasons. First, because interaction between two turbulent fields is likely to depend upon the spectral distribution of each. And, secondly, because the free-stream turbulence is also affected by the constraint of zero normal velocity at a solid surface, the effect of which has been shown to extend approximately one free-stream lengthscale from the wall (Thomas & Hancock 1977. This latter effect does not occur in free-shear layers affected by free-stream turbulence.) Mean-flow parameters such as wall shear stress and wake strength correlate well with a purely empirically devised parameter $\beta = (u'/U)_e/(L_e^u/\delta_{995}+2)$ which also appears adequate to correlate some aspects of the change in turbulence structure. In the outer layer the structure is changed substantially, while the main effect in the inner layer is increased inactive motion and increased diffusion of kinetic energy and shear stress away from the wall. Nevertheless, the larger diffusion is small compared with generation and destruction, so that local equilibrium results like the logarithmic law are still trustworthy, as is suggested by the observed universality of the velocity profile gradients.

The conditionally sampled measurements were particularly valuable. The intermittency profile is substantially affected both in its standard deviation and its mean position, the latter depending primarily on the free-stream lengthscale, and the former confirming intuition and flow visualization observations of increased mixing of a smoke-filled boundary layer. Structural parameters based upon contributions from the hot-zone fluid to the Reynolds stresses and to the turbulent transport of Reynolds stresses (i.e. triple-velocity products), though markedly affected, are more comparable with those when free-stream turbulence is absent than are their conventionally averaged counterparts. Significantly, larger free-stream lengthscales penetrate further into the boundary layer even though the effect on the mean flow is less. The finding that the effect on the hot-zone shear-stress correlation coefficient is also less suggested that the hot-zone motions are principally affected by the fluctuating-strain rate imposed by the intruding cold-zone motions. These intruding

motions are predominantly large-scale motions, and it was argued that the mean effect of the fluctuating-strain rate should scale upon the parameter $e = u'_e\delta_{995}/(U_e L^u_e)$, and that the change in the cold-zone structure should be correlated by the same parameter. The argument has been confirmed by the systematic behaviour with e of several structural parameters, some of which have been included here. In the Reynolds-stress transport equations the interaction is presumably via the pressure–strain term, predominantly in the energy-containing wavenumber range.

Apart from the increase in turbulent diffusion from the inner layer, mentioned above, the most noticeable feature of the turbulent energy and shear-stress balances is the lack of effect of free-stream turbulence on the dissipation length parameter L_τ, which provides some support for the qualitative feeling that, at least in the presence of free-stream turbulence, the shear stress provides a more meaningful velocity scale for the boundary-layer turbulence than does the turbulent intensity as such.

REFERENCES

ANDREOPOULOS, J. & BRADSHAW, P. 1980 Measurements of interacting turbulent shear layers in the near wake of a flat plate. *J. Fluid Mech.* **100**, 639–668.

BLAIR, M. F. 1983 Influence of free-stream turbulence on turbulent boundary layer heat transfer and mean profile development. *Trans. ASME* C: *J. Heat Transfer* **105**, 33–40 and 41–47.

BLAIR, M. F. & EDWARDS, D. E. 1982 The effects of free-stream turbulence on the turbulence structure and heat transfer in zero pressure gradient boundary layers. *United Technologies Research Center, Rep.* R82-915634-2.

BRADSHAW, P., FERRISS, D. H. & ATWELL, N. P. 1967 Calculation of boundary-layer development using the turbulent energy equation. *J. Fluid Mech.* **28**, 593–616.

BROWN, G. L. & THOMAS, A. S. W. 1977 Large structures in a turbulent boundary layer. *Phys. Fluids* **20**, s243–s252.

CASTRO, I. P. 1984 Effects of free-stream turbulence on low Reynolds number boundary layers. *Trans. ASME* I: *J. Fluids Engng* **106**, 298–306.

CHARNAY, G., MATHIEU, J. & COMTE-BELLOT, G. 1976 Response of a turbulent boundary layer to random fluctuation in the external stream. *Phys. Fluids* **19**, 1261–1272.

COLES, D. 1956 The law of the wake in the turbulent boundary layer. *J. Fluid Mech.* **1**, 191–226.

DEAN, R. B. & BRADSHAW, P. 1976 Measurement of interacting turbulent shear layers in a duct. *J. Fluid Mech.* **78**, 641–676.

HANCOCK, P. E. 1980 The effect of free-stream turbulence on turbulent boundary layers. PhD thesis, Imperial College, London.

HANCOCK, P. E. & BRADSHAW, P. 1983 The effect of free-stream-turbulence on turbulent boundary layers. *Trans. ASME* I: *J. Fluids Engng* **105**, 284–289.

HANCOCK, P. E. & BRADSHAW, P. 1987 The structure of a turbulent boundary layer beneath a turbulent free stream. *Proc. 6th Symp. Turbulent Shear Flows, Toulouse, France. Paper* 1–1.

HEDLEY, B. T. & KEFFER, J. F. 1974*a* Turbulent/non-turbulent decisions in an intermittent flow. *J. Fluid Mech.* **64**, 625–644.

HEDLEY, B. T. & KEFFER, J. F. 1974*b* Some turbulent/non-turbulent properties of the outer intermittent region of a boundary layer. *J. Fluid Mech.* **64**, 645–678.

HUNT, J. C. R. & GRAHAM, J. M. R. 1978 Free-stream turbulence near plane boundaries. *J. Fluid Mech.* **84**, 209–235.

KLEBANOFF, P. S. 1955 Characteristics of turbulence in a boundary layer with zero pressure gradient. *NACA Rep.* 1247.

KOVASZNAY, L. S. G., KIBENS, V. & BLACKWELDER, R. F. 1970 Large-scale motion in the intermittent region of a boundary layer. *J. Fluid Mech.* **41**, 283–325.

RODI, W. & SCHEUERER, G. 1985 Calculation of turbulent boundary layers under the effect of free-stream turbulence. *Proc. 5th Symp. Turbulent Shear Flows, Cornell University*, pp. 2.19–2.25.

THOMAS, N. H. & HANCOCK, P. E. 1977 Grid turbulence near a moving wall. *J. Fluid Mech.* **82**, 481–496.

UZKAN, T. & REYNOLDS, W. C. 1967 A shear-free turbulent boundary layer. *J. Fluid Mech.* **28**, 803–821.

WEIR, A. D., WOOD, D. H. & BRADSHAW, P. 1981 Interacting turbulent shear layers in a plant jet. *J. Fluid Mech.* **107**, 237–260.